Size Dependence of Pt Catalysts for Propane Dehydrogenation: From Atomically Dispersed to Nano Particles

Wei Zhang,[‡,†] Haizhi Wang,[‡,†] Jiawei Jiang,[†] Zhijun Sui,*[,†] Yian Zhu,[†] De Chen,*[,§] Xinggui Zhou[†]

[†]State Key Laboratory of Chemical Engineering, East China University of Science and Technology, 130 Meilong Road, Shanghai 200237, China

[§]Department of Chemical Engineering, Norwegian University of Science and Technology, Trondheim 7491, Norway

KEYWORDS: Propane dehydrogenation; Size effects; Platinum catalyst; Atomically dispersed; Coking

ABSTRACT: The structure–performance relationship is a critical fundamental issue in heterogeneous catalysis, and the size-dependent structure sensitivity of catalytic reactions has long been researched in catalysis. Yet it mains elusive for most of the reactions in a full-size range, from a single atom and subnanometer clusters to nanoparticles. Herein we report a complete size dependence of Pt catalytic performed in propane dehydrogenation in terms of activity, selectivity, and stability due to coke formation. The TOF of the atomically dispersed Pt/Al2O3 catalyst was approximately 3-fold and 7-fold higher than the subnanometer sized clusters and the nanoparticles, respectively. A canyon shape of size dependence of the propene selectivity was observed with a bottom at about 2 nm. The subnanometer sized clusters have an opposite size dependence of the propene selectivity compared to nanoparticles. Both atomically dispersed Pt and large Pt nanoparticle possess high propene selectivity. The atomically dispersed platinum centers with positive charge dramatically enhanced the activity, weakened propylene adsorption and prevented its deep dehydrogenating. Besides, the absence of multiple Pt-Pt sites effectively inhibited undesired side reactions (e.g. C-C cracking), thus improved propylene selectivity and stability. This work demonstrates the promising application of supported atomically dispersed Pt catalyst for highly selective dehydrogenation of propane.

INTRODUCTION

Propane dehydrogenation (PDH) has become an important alternative as a result of the ever-increasing demand for propylene hardly being met by traditional methods of propene production, e.g., steam cracking and fluid catalytic cracking.[1-4] Noble Pt is widely used as active components in PDH due to its superior activity. Nevertheless, their selectivity to propylene is not entirely satisfactory.[5,6] To address the problem, Sn is typically added as a promoter for monometallic Pt catalyst to enhance propylene selectivity in industry process,[7,8] but Zhu et al.[9] reported that alloying Pt with Sn significantly lowers the reaction rate of PDH. Besides, the gradual catalyst deactivation owing to the formation of coke remains an insuperable issue.[10-13] Therefore, the critical requirements in PDH are (1) to minimize noble Pt usage for lowering production costs; (2) to maintain high propylene selectivity at high levels of activity; (3) to increase anti-coking ability.

Great efforts have been devoted to improve the activity and stability of Pt catalysts, and it shows that the Pt particle size and catalyst support are all proposed to have a significant impact on catalytic performance.[14-18] Propane dehydrogenation is a fully known structure sensitive reaction. Zhu et al.[19] illustrate the catalytic activity on Pt nanoparticles increases when decreasing the particle size in the range of 1-9 nm, while the propylene selectivity behaves in the opposite way. According to analysis, the smaller Pt nanoparticles dominated by Pt(211) faces reveal a lower dehydrogenation energy barrier and thus more reactive for propane conversion, but large Pt nanoparticles dominated by Pt(111) faces exhibit a higher energy barrier for C-H bond activation and a weaker binding strength of propylene.[20,21]

In recent years, with the fabrication of single-atom catalysts establishing a new frontier in heterogeneous catalysis, in-depth research into catalysts has been performed at a smaller size scale.[22-27] Numerous studies suggest that single-atom catalysts could not only minimize noble metal usage but could also frequently exhibit more outstanding catalytic properties in a broad area of chemical reactions, such as CO oxidation,[28,29] selective hydrogenation,[28,30] water-gas shift reaction,[31,32] methanol steam reforming,[33] electrochemical reactions[34,35] and so on. Single-atom catalysts are providing new approaches for designing desired propane dehydrogenation catalysts with both high activity and selectivity. Gong et al.[36] synthesize γ-Al_2O_3-supported Pt/Cu single-atom catalysts for PDH through a copper atom dilution method. Pt single atoms dispersed on Cu nanoparticles dramatically enhance the desorption of surface-bonded propylene and prohibit its further dehydrogenation, displaying propylene selectivity of ~90%, but there is a slight loss of intrinsic dehydrogenation activity. Furukawa et al.[37] report that the PtGa-Pb/SiO_2 catalyst as a stable and selective catalyst for PDH, in which threefold hollow Pt_3 ensembles are selectively blocked and disabled by Pb deposition, while single-atom Pt_1 sites isolated by catalytically inert Ga at the surface. The Pt_3 site is considered more active for further C-H(C) scissions, so Pt3 sites should be disabled while Pt1 sites available for the reaction are needed to achieve higher selective and stable. Zhao et al.[38] adopt the different doped graphene strategy tune the electronic structure of supported Pt atom in a wide range. The single Pt with the most positive charges is predicted to be the most active and less prone to happen deep dehydrogenation by using first-principles calculations. A wide range of research has proved that, when the size of metal particle reduces to subnanometer or atomic dispersed, it typically manifests the unique catalytic properties differing from the conventional nano-catalysts owing to the exclusive structural and electronic attribution. Therefore, it is necessary to systematically study the size effects on the catalytic performance from single atoms to small clusters and then

to nanoparticles, gaining a better understanding of the structure-performance relationship and thus design better industrial catalysts.

Herein, a series of Al_2O_3-supported Pt single atoms, small-clusters, and nanoparticle catalysts were prepared via a simple impregnation method in which the Pt particle size could be controlled by way of changing the Pt loading. The properties of Pt species at different scales were detailed characterized by HAADF-STEM, CO-Chem, XPS and diffuse reflectance infrared Fourier transform spectroscopy (DRIFTS) of CO adsorption. The size effects of Pt particles on catalytic performer was explored. Combining kinetic analysis and DRIFTS of C_3H_6 chemisorption gave the relative adsorption strength of surface species on multimetric Pt species, which relates to reactivity and selectivity. Moreover, the size effects on coke properties have been completely developed for the first time. The comprehensive information on coke formed on multimetric Pt catalysts was qualitatively and quantitatively determined by HRTEM, GC-MS, and TG using different carrier gases. A combined catalyst characterization and kinetic study reveal the underlying nature of the structure-performance relationship. The Al_2O_3-supported atomically dispersed Pt catalyst is a novel catalyst with a high precious atom efficiency and excellent catalytic dehydrogenation ability, selectivity, and stability.

EXPERIMENTAL

Catalyst Preparation. In the present study, the hierarchically structured nano-alumina was chosen as Pt catalyst support to investigate the Pt particle size effect. Compared with commercial alumina, the hierarchical nano-alumina benefited from its highly open structure, and stable surface property showed a remarkable ability to improve the mass-transfer, diffusion kinetics, and catalyst's structural stability.[39] The Al_2O_3 support material was synthesized by a hydrothermal method described earlier.[40] 8.4 g $Al(NO_3)_3{\cdot}9H_2O$ (Sinopharm Chemical Reagent Co. Ltd, 99.5%) and 6 g urea (Sinopharm Chemical Reagent Co. Ltd, 99.5%) were dissolved in 50 mL water-ethanol mixture followed by the addition of an appropriate amount of nitric acid with vigorous stirring at room temperature. The mixed solution was transferred into a 100 mL Teflon-lined stainless autoclave and heated at 180 °C for 12 h under autogenous pressure. The precipitate was dried at 80 °C for 12 h after washing and filtering, and finally calcined in air at 900 °C for 3 h with a heating rate of 10 °C/min.

All the supported Pt catalysts were prepared by the incipient-wetness impregnation method. Typically, an aqueous solution of $H_2PtCl_6{\cdot}6H_2O$ (Sinopharm Chemical Reagent Co. Ltd, 99.5%) was added dropwise onto 1.00 g of supports under manual stirring. After the impregnation, the samples were dried at 110 °C for 12 h and then calcined at 500 °C for 3 h with a heating rate of 2 °C/min in air, as unreduced catalyst precursors. For the Al_2O_3 support, appropriate amounts of Pt were used to give nominal loadings of 0.05 wt%, 0.1 wt%, 0.3 wt%, 0.5 wt%, 1 wt%, 3 wt% and 5 wt%, which were denoted as 0.05% Pt/Al_2O_3, 0.1% Pt/Al_2O_3, 0.3% Pt/Al_2O_3, 0.5% Pt/Al_2O_3, 1% Pt/Al_2O_3, 3% Pt/Al_2O_3 and 5% Pt/Al_2O_3. To increase the particle size and ensure practically no single atoms, the samples with 5 wt% Pt loading were calcined at 600 °C and at 700 °C for 3 h with a heating rate of 2 °C/min in air, respectively, which were denoted as 5% Pt/Al_2O_3-600 and 5% Pt/Al_2O_3-700.

Catalyst Characterization. N_2 adsorption/desorption isotherms were performed on a Micromeritics ASAP 2010 instrument at -196 °C, with all samples degassed in vacuum for 4 h at 240 °C. The samples' surface areas were analyzed by the multipoint BET analysis method in the P/P_0 = 0.05-0.30 pressure range. An inductively coupled plasma atomic emission spectrometer (ICP-AES, Agilent Varian 710-ES, USA) was applied to analyze the Pt contents. X-ray photoelectron spectroscopy (XPS) was performed on a Thermo Scientific Escalab 250Xi spectrometer equipped with Al Kα ($h\nu$=1486.71 eV) radiation source. The binding energy was calibrated using the C 1s peak (284.6 eV) of surface adventitious carbon. The transmission electron microscopy (TEM) images and were collected with a JEOL JEM-2100 transmission electron microscope with an acceleration voltage of 200 kV. The aberration-corrected high-angle annular dark-field scanning transmission electron microscopy (HAADF-STEM) was performed on JEOL JEM-ARM200F at 200 kV to obtain atomic resolution imaging. The surface-averaged Pt cluster diameters (d_{TEM}) were determined on the basis of more than 150 particles in different regions of TEM images. The thermogravimetric analysis (TG) was performed on PerkinElmer Pyris 1 TGA instrument to determine the amount of coke, in the oxygen and nitrogen atmosphere. The sample was dried at 120 °C for 2 h, and then the temperature increased to 800 °C at a heating rate of 10 °C/min. The chemical composition of the coke was analyzed by pyrolysis GC-MS (Agilent 7890A GC/5975C MSD) equipped with an HP-5MS column, as reported in our previous work.[10]

CO chemisorption (CO-Chem) and H_2 temperature-programmed desorption (H_2-TPD) were carried out using an Autochem-II 2920 analyzer (Micromeretics, USA) equipped with a thermal conductivity detector (TCD). For CO-Chem, approximately 0.20 g catalyst was loaded into a U-shaped quartz tube and heated to 550 °C for 100 min under pure H_2 (20 mL/min) and then cooled to 45 °C in pure Ar (20 mL/min), and then CO pulses (10% CO/Ar) were injected to begin testing. The dispersion of platinum was estimated by CO chemisorption amount assuming the adsorption stoichiometry of CO/Pt=1. For H_2-TPD, approximately 0.2 g catalyst was reduced in the same way as CO chemisorption. The catalyst was kept under flowing pure H_2 for 1 h. After saturation, a flow of He was used to remove the weakly adsorbed H_2 on the catalysts and then the TPD process was carried out from 45 to 600 °C at a ramp rate of 10 °C/min.

In situ diffuse reflectance infrared Fourier transform spectra of CO (CO-DRIFTS) and C_3H_6 (C_3H_6-DRIFTS) adsorbed on catalysts were acquired with PerkinElmer Spectrum 100 FTIR spectrometer equipped with liquid nitrogen cooled MCT detector at a spectral resolution of 4 cm^{-1} and the scanned wave number was ranged from 4000 to 400 cm^{-1}. In a typical CO-DRIFTS procedure, about 50 mg sample was reduced at 550 °C in pure H_2 (20 ml/min) for 100 min and then cooled to 30 °C under pure Ar (20 ml/min) for collecting a background spectrum. Afterward, 2% v/v CO/Ar (20 ml/min) was introduced for 30 min to ensure steady-state conditions. An Ar (20 mL/min) purge was performed to remove gas-phase CO from the DRIFTS cell and then spectra of chemisorbed CO were recorded continuously during the process. For C_3H_6-DRIFTS, the sample was reduced in the same manner as that for CO adsorption. The sample was exposed to pure C_3H_6 (20 mL/min) at 30 °C for 30 min and subsequently purged with Ar (20 mL/min) for 30 min, and then the spectra were collected for analysis. Afterward, the sample was elevated to 100, 200, and 300 °C in Ar (20 mL/min), respectively. The previous step was repeated to obtain spectra under different temperatures.

Catalytic Evaluation. The propane dehydrogenation reaction was carried out on a BenchCAT reactor (Altamira Instrument, USA) under 1 bar. Typically, 0.10 g catalyst was loaded in the center of a quartz tube with an inner diameter of 6 mm, and reduced at 500 °C in flowing pure H_2 (20 mL/min) for 100 min with a heating rate of 10 °C/min. After that, syngas (H_2/C_3H_8=0.8 v/v, Argon balance, 78 mL/min) was introduced to the reactor, which give a $WHSV_{propane}$ =18.9 h^{-1}, and the catalyst was tested at 575 °C for 4 h. The analysis of reactant and product components was performed with an online gas chromatograph equipped with a TCD detector (INFICON 3000, USA). The conversion of propane, selectivity toward propylene were calculated as:

$$Conversion = \frac{F_{C_3H_8,in} - F_{C_3H_8,out}}{F_{C_3H_8,in}} \times 100\%$$

$$Selectivity = \frac{F_{C_3H_6,out}}{\sum_i \frac{n_i}{3} F_{i,out}} \times 100\%$$

Here, $F_{C_3H_8,in}$ is the flow rate of propane in the feed; $F_{C_3H_8,out}$, $F_{C_3H_6,out}$, and $F_{i,out}$ are the flow rates of propane, propylene, and component *i* in the outlet; n_i is the carbon number of component *i*.

The diffusion free operation was examined experimentally by varying space velocities and catalyst particle sizes. Results showed that the external and internal diffusion effects were safely excluded under the reaction conditions adopted here. The turnover frequency (TOF) was calculated as:

$$TOF = \frac{(F_{in} - F_{out})M}{mLD}$$

Here, F_{in} is the molar flow rate of propane in the feed (mol/s) ; F_{out} is the molar flow rate of propane in the outlet (mol/s); *M* is the molar mass of Pt (g/mol); *m* is the amount of catalyst (g); *L* is the loading amount of Pt (%); *D* is the dispersion of Pt (%), estimated by CO chemisorption. The initial values of the reactions were used.

RESULTS AND DISCUSSION

Morphology and Structure of Supported Catalysts. Table 1 lists the detailed properties of the alumina supported Pt catalysts. The final loadings of Pt were analyzed by ICP-AES are close to the nominal values. The surface areas and pore volumes of catalysts with different loading are 60.3-68.7 m^2/g and 0.31-0.36 cm^3/g, respectively. Following the improvement of Pt loading, it was noticed that there was a slight decrease in specific surface and pore volume, but the structural properties of the Al_2O_3 support materials were unchanged during the catalyst preparation process. The Pt dispersions determined by CO chemisorption are on the decline along with the Pt loading increasing. The 0.05% Pt/Al_2O_3 and 0.1% Pt/Al_2O_3 exhibit superb 98% and 97% dispersion, respectively, indicating that Pt particles on support are highly dispersed.

The Pt particle sizes determined by HAADF-STEM images (Figure 1) are also shown in Table 1. No obvious changes in Pt particle size (Table 1) were found after PDH reaction, which means no sintering happened on these Pt catalysts under the reaction conditions, and there is good interaction between the Al_2O_3 support and the Pt particles.

It can be seen from Figure 1a, when a small amount of Pt as low as 0.1%, it is difficult to obtain the images of Pt particle on support at low magnification. However, as the magnification increases, Figure 1b displayed a great deal of the presence of brighter single Pt atoms on the Al_2O_3 support, some of which are loosely packed to disordered Pt aggregates. Remarkably, Pt particles on 0.1% Pt/Al_2O_3 are not all completely isolated, but the Pt aggregates appear to be amorphous instead of crystallites with clear edges, the dispersion of which is atomic-level. Following an increase of the Pt loading to 0.3 wt%, even at low magnification, a considerable number of Pt particles can be observed, and the average diameters are ~0.8 nm, as shown in Figure 1c. After the magnification (Figure 1d), the 0.3% Pt/Al_2O_3 catalyst exhibits intermediate features. These contain many small clusters (~ 1 nm) with ordered Pt atoms, accompanied by sporadic single Pt atoms.[34,41] The HRTEM image of 3% Pt/Al_2O_3 (Figure 1f) reveals many well-defined crystalline particles spread on the support, where continuous lattice fringes are observed. Combining the corresponding Fourier transform (FFT) pattern, the lattice spacings of nanoparticles in 3% Pt/Al_2O_3 are 0.224 nm and 0.198 nm. These values are very close to the d-spacing of Pt(111) planes and Pt(100) planes (JCPDS 04-0802), respectively. The size of 5% Pt/Al_2O_3-600 and 5% Pt/Al_2O_3-700 that was thermal treated grow to ~6.9 nm and ~12 nm, respectively. The $d_{CO\text{-}Chem}$ calculated on the basis of CO chemisorption are found to be consistent with the size measured by HAADF-STEM. According to these results, the Pt/Al_2O_3 catalysts in multiscale (from atomically dispersed to small clusters and nanoparticles) were successfully prepared using the impregnation method.

The Size Effects on Catalytic Performance. The performance of propane dehydrogenation on Pt/Al_2O_3 catalysts with different Pt sizes was investigated (Figure 2a,b), and the relationship between particle size and catalytic performance was plotted in Figure 2c. The size dependence of catalysts activity, selectivity, and stability can be categorized into three regions. In the first region, the atomically dispersed 0.05% Pt/Al_2O_3 and 0.1% Pt/Al_2O_3 catalysts have the highest activity, propene selectivity and stability for propane conversion, where TOF reaches 4.65 and 4.25 s^{-1}, respectively. Meanwhile, the propylene selectivity is higher than 92%, which is very high for Pt monometallic catalyst with high activity in PDH. As shown in Figure 2d, the performance of 0.1% Pt/Al_2O_3 is greater than that of the majority of the supported Pt-based catalysts reported recently.[18,19, 41-57] In the second region with relatively low loading and Pt existed as the small clusters from 0.8 to 2 nm, the activity, propene selectivity, and stability decreased with increasing the cluster size. As the Pt loading increased from 0.1% to 0.3% and the Pt size increases from the atomically dispersed to ~0.8 nm small clusters, the catalytic performance has dramatically changed. The TOF decreased almost three times (from 4.25 s^{-1} to 1.48 s^{-1}), and the propene selectivity also decreased from 92% to 85%. In the third region where Pt existed as nanoparticles, the activity (TOF) decreased with increasing the particle size, while the propene selectivity and stability increased with increasing the Pt particle size, which is in agreement with the reported nanoparticle size dependence of the catalytic performance.[19] The Pt/Al_2O_3 catalyst (3%) with the 2 nm size exhibits the lowest propylene selectivity (53%), and the main byproducts are C-C bond cracking products, i.e., methane, ethylene, and ethane.

Table 1. Physical properties of Pt/Al_2O_3 catalysts.

Sample	Pt loading[a] (wt%)	S_{BET}[b] (m^2/g)	V_P[b] (cm^3/g)	Pt dispersion[c] (%)	$d_{CO\text{-}Chem}$ (nm)	d_{TEM}[d] (nm)	d_{TEM}[e] (nm)
Al_2O_3	-	68.7	0.36	-	-		
0.05% Pt/Al_2O_3	0.05	68.2	0.35	98%	-		
0.1% Pt/Al_2O_3	0.10	67.8	0.35	97%	-	-	
0.3% Pt/Al_2O_3	0.28	66.1	0.36	89%	1.2	0.8 ± 0.2	0.9 ± 0.2
0.5% Pt/Al_2O_3	0.46	67.1	0.33	85%	1.3	1.2 ± 0.2	1.3 ± 0.2
1% Pt/Al_2O_3	0.94	62.8	0.32	70%	1.6	1.4 ± 0.3	1.5 ± 0.3
3% Pt/Al_2O_3	2.90	61.3	0.33	45%	2.4	2.0 ± 0.4	2.2 ± 0.4
5% Pt/Al_2O_3	4.89	60.5	0.31	41%	2.7	2.6 ± 0.6	2.7 ± 0.6
5% Pt/Al_2O_3-600[f]	4.87	62.3	0.33	14%	7.8	6.9 ± 3	7.1 ± 3
5% Pt/Al_2O_3-700[g]	4.84	60.3	0.32	7.8%	14.4	12.0 ± 4	12.4 ± 4

[a] Determined by ICP-AES. [b] Calculated from N_2 adsorption/desorption experiments. [c] Determined by CO chemisorption at 45 °C with assuming CO/Pt = 1. [d] Supported Pt catalysts, after PDH reaction, characterized by TEM (Figure 1). [e] Supported Pt catalysts, after 4 h PDH reaction, characterized by TEM (Figure 8). [f,g] The samples were heat treated.

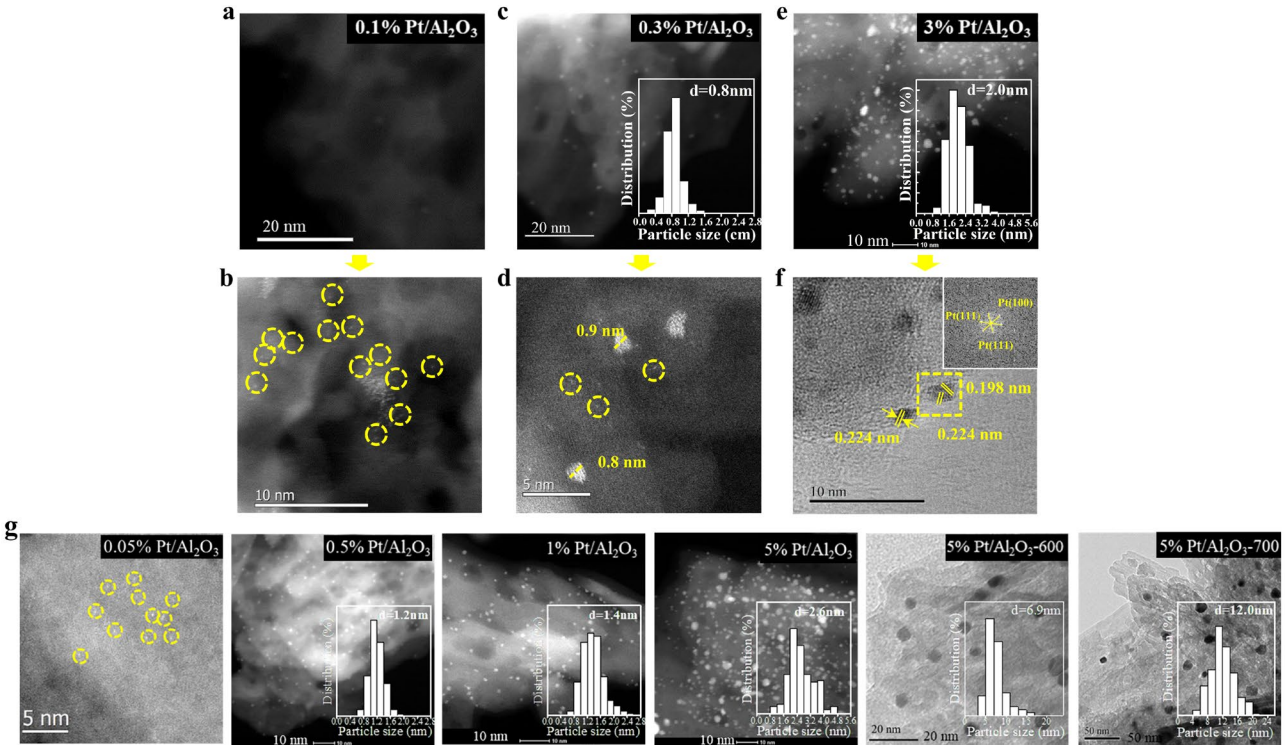

Figure 1. Typical HAADF-STEM images and particle size distributions of fresh catalysts of (a) 0.1% Pt/Al_2O_3, (c) 0.3% Pt/Al_2O_3, (e) 3% Pt/Al_2O_3 at low magnification, and (b) 0.1% Pt/Al_2O_3, (d) 0.3% Pt/Al_2O_3 at high magnification. HRTEM image of (f) 3% Pt/Al_2O_3 and FFT pattern. (g) Typical HAADF-STEM images of 0.05% Pt/Al_2O_3, 0.5% Pt/Al_2O_3, 1% Pt/Al_2O_3 and 5% Pt/Al_2O_3, and typical TEM images of 5% Pt/Al_2O_3-600 and 5% Pt/Al_2O_3-700. Single Pt atoms are marked by yellow circles.

To exclude the possible effect of conversion on the selectivity, the propylene selectivity was rigorously compared at the similar conversion of propane in Figure 2e,f, which shows the similar size dependence, as shown in Figure 2c. Additionally, the stability index is related to the coke formation, and it follows a similar trend of the size dependence of the propene selectivity. As shown in Figure 2c, the conversion loss of the atomically dispersed Pt (0.05% and 0.1%) is minimum during the reaction, showing good stability. In conclusion, the atomically dispersed Pt/Al_2O_3 catalyst has an outstanding catalytic activity while still retaining a high propylene selectivity and stability, and the TOF is approximately 3-fold and 7-fold higher than small clusters and nanoparticles, respectively.

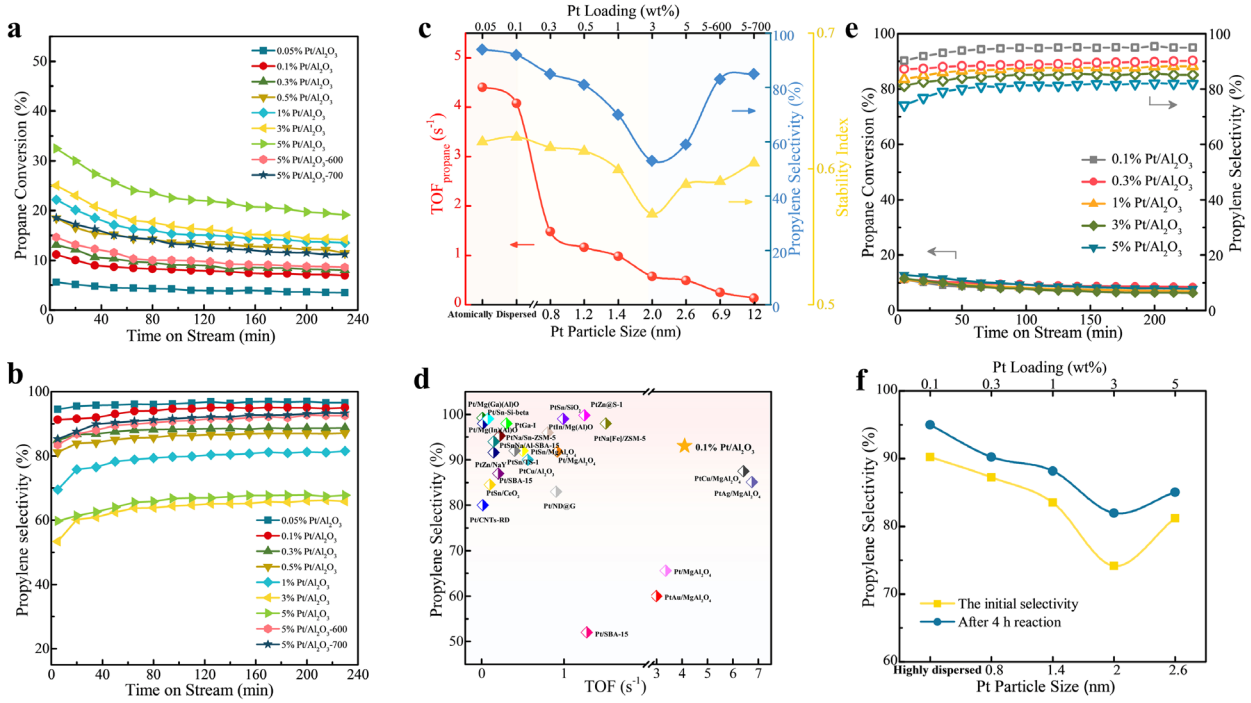

Figure 2. (a) Propane conversion and (b) propylene selectivity over Pt/Al_2O_3 catalysts with different Pt loading. Reaction conditions: 0.1 g catalyst, P = 1 atm, T = 575 °C, and H_2/C_3H_8=0.8 v/v, Argon balance, V_{toltal}=78 mL/min, $WHSV_{propane}$ =18.9 h^{-1}. (c) Comparison of the initial $TOF_{propane}$ and selectivity of catalysts of different Pt particle sizes (Pt loadings). The Pt particle size was measured by HAADF-STEM. The stability index was defined as the ratio of the final conversion to the initial conversion. (d) Comparison of $TOF_{propane}$ and selectivity of 0.1% Pt/Al_2O_3 catalyst and other reported Pt-based catalysts. The value is obtained at the start of the cycle. (e) Comparison of the propylene selectivity of Pt/Al_2O_3 catalysts with different Pt loading under similar propane conversion. (f) Comparison of the initial and final selectivity of catalysts of Pt/Al_2O_3 catalysts in different sizes (loadings).

The Nature of the Size Dependence. The catalytic performance of a catalyst generally depends on the geometric and electronic structure of active sites. XPS characterization of the three typical Pt/Al_2O_3 at different scales were carried out to illustrate the electronic properties modification by Pt particle size. The most intense photoemission line of Pt was arising from the Pt 4f, but this energy region was overshadowed by the presence of a very strong Al 2p peak, and so the Pt 4d was analyzed.[58,59] As shown in Figure 3, the peaks of the three catalysts could be resolved into three components with binding energies (B.E.) of 317.0-317.5, 314.9-315.3 and 312.2-312.9 eV after curve fitting procedures, assigned to the presence of Pt^{4+}, Pt^{2+} and Pt^{0+} species, respectively.[60] The detailed curve-fitting parameters from XPS are listed in Table 2. Clearly, as the Pt loading decreases, a shift of the Pt $4d_{5/2}$ B.E. towards higher values and the proportion of oxidized $Pt^{\delta+}$ species gradually increased. The results demonstrate a stronger interaction which gradually grows with decreasing the Pt loading between the Pt and supports, and the Pt particles in 0.1% Pt/Al_2O_3 can transfer additional charge to the support compared to 0.3% Pt/Al_2O_3 and 3% Pt/Al_2O_3, this implies that the atomically dispersed Pt atoms contain more positive charges than small clusters and nanoparticles.

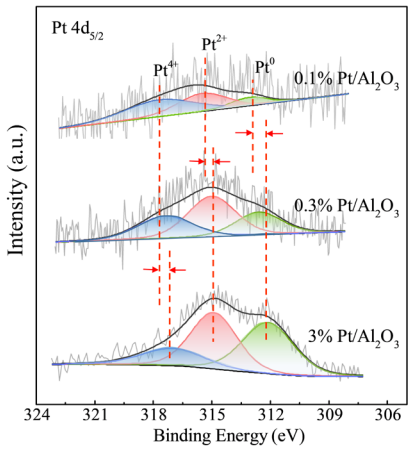

Figure 3. Pt $4d_{5/2}$ XPS spectra of fresh Pt/Al_2O_3 with different loading.

Table 2. Curve-fitting parameters for Pt $4d_{5/2}$ XPS spectra of fresh catalysts.

Sample	Binding Energy (eV)		
	Pt^{4+}	Pt^{2+}	Pt^{0+}
0.1% Pt/Al_2O_3	317.6 (45%)	315.4 (46%)	312.9 (9%)
0.3% Pt/Al_2O_3	317.4 (29%)	315.0 (44%)	312.6 (27%)
3% Pt/Al_2O_3	317.0 (17%)	314.9 (41%)	312.2 (42%)

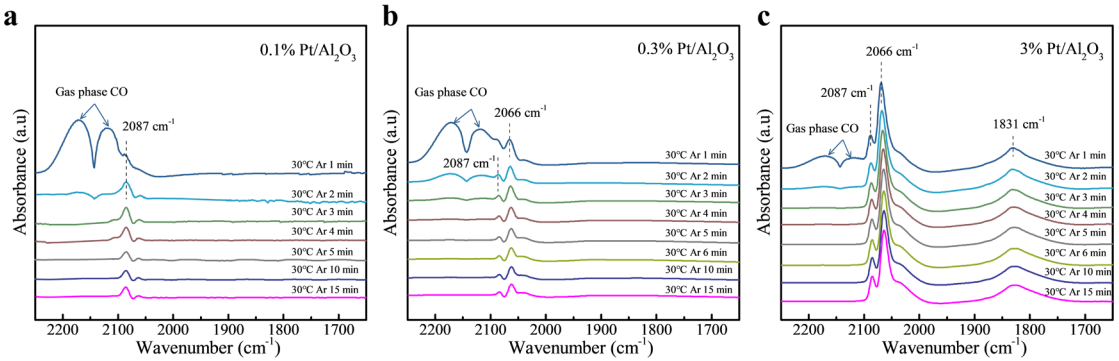

Figure 4. DRIFTS of CO adsorption on (a) 0.1% Pt/Al_2O_3, (b) 0.3% Pt/Al_2O_3 and (c) 3% Pt/Al_2O_3 catalysts

The FT-IR spectroscopy is a powerful site-specific characterization method that can be used to accurately identify Pt species in a catalyst sample. As shown in Figure 4, when Pt particle sizes decrease to the small cluster levels, two bands at 2087 cm^{-1} and 2066 cm^{-1} can be assigned to the linear-bonded CO on single $Pt^{\delta+}$ and Pt^0 atoms, respectively and no bridged adsorbed CO was observed.[28,31] For 0.1% Pt/Al_2O_3, the Pt species exist privileged as single $Pt^{\delta+}$ atoms, while the peaks of the linear-bonded CO on Pt^0 is more obvious for 0.3% Pt/Al_2O_3. For Al_2O_3 supported Pt nanoparticles, the CO adsorption bands at 1950 to 2100 cm^{-1} are usually assigned to the linear-bonded CO on metallic nanoparticle surfaces at either well-coordinated (2080~2090 cm^{-1}) or under-coordinated (2030~2070 cm^{-1}) Pt sites. Meanwhile, the band at 1831 cm^{-1} is observable on 3% Pt/Al_2O_3, which is assigned to the bridged CO species adsorbed on neighboring Pt atoms over the well-defined Pt crystallite.[61] These characterizations collectively provide compelling evidence that 0.1% Pt/Al_2O_3 and 3% Pt/Al_2O_3 are dominated by positively charged $Pt^{\delta+}$ atoms and well-defined Pt metallic crystallite, respectively, while 0.3% Pt/Al_2O_3 exhibits the intermediate features of a large number of small clusters and a small amount of single Pt atoms.

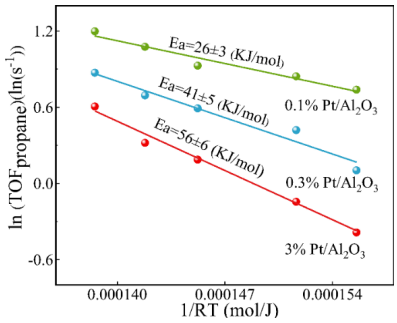

Figure 5. Apparent activation energy of propane dehydrogenation over multimetric Pt/Al_2O_3 catalysts. Apparent activation energy was calculated under a low propane conversion (<10%).

Furthermore, the kinetic study was performed to elucidate the size dependence of the kinetic behaviors and the Arrhenius plots for PDH on the atomically dispersed Pt (0.1% Pt/Al_2O_3), small clusters (0.3% Pt/Al_2O_3) and nanoparticles (3% Pt/Al_2O_3) are presented in Figure 5. The activation energy (E_a) were calculated by the Arrhenius equation:

$$k = Aexp(-\frac{E_a}{RT}) \quad (1)$$

where A, R and T are the pre-exponential factor, universal gas constant and absolute temperature, respectively.

The activation energy for PDH over 3% Pt/Al_2O_3 nano-catalyst is 56 ± 6 kJ/mol, and decreased to 41 ± 5 kJ/mol on small clusters and 26 ± 3 kJ/mol on atomically dispersed Pt. This result further confirms that the atomically dispersed Pt particles are more conducive to the improvement of reaction rate.

The entropy of activation can effectively demonstrate the change between the transition state of propane activation and the gas phase propane, where the entropy loss of the propane adsorption on the Pt surface due to the loss of freedom contributes mainly to the apparent entropy changes. Based on the transition state theory, the reaction rate (k) can be expressed in the Eyring form: [9, 62,63]

$$k = \frac{k_B T}{h} exp\,(\frac{\Delta S^{0*}}{R}) exp\,(-\frac{\Delta H^{0*}}{RT}) \quad (2)$$

where k_B, T, h, ΔS^{0*}, R and ΔH^{0*} are the Boltzmann constant, absolute temperature, Planck constant, entropy of activation, universal gas constant and enthalpy of activation, respectively.

The activation energy could be related to ΔH^{0*}:

$$E_a = \Delta H^{0*} + nRT \quad (3)$$

where n is the molecularity of reaction (Herein, n=1).

Combining Eqs. (1), (2), (3) gives

$$A = \frac{k_B T}{h} e^n exp\,(\frac{\Delta S^{0*}}{R}) \quad (4)$$
$$= \frac{k_B T}{h} e \cdot exp\,(\frac{\Delta S^{0*}}{R})$$

The pre-exponential factors were obtained from the Arrhenius plots, and then the apparent entropy changes were also estimated based on Eq. (4). As shown in Table 3, the larger entropy change of 0.1% Pt/Al_2O_3 indicates the stronger adsorption of the propane on 0.1% Pt/Al_2O_3 compared to 0.3% Pt/Al_2O_3 and 3% Pt/Al_2O_3. Therefore, reactant species might favour preferential adsorption on 0.1% Pt/Al_2O_3, which enhances overall reactivity.

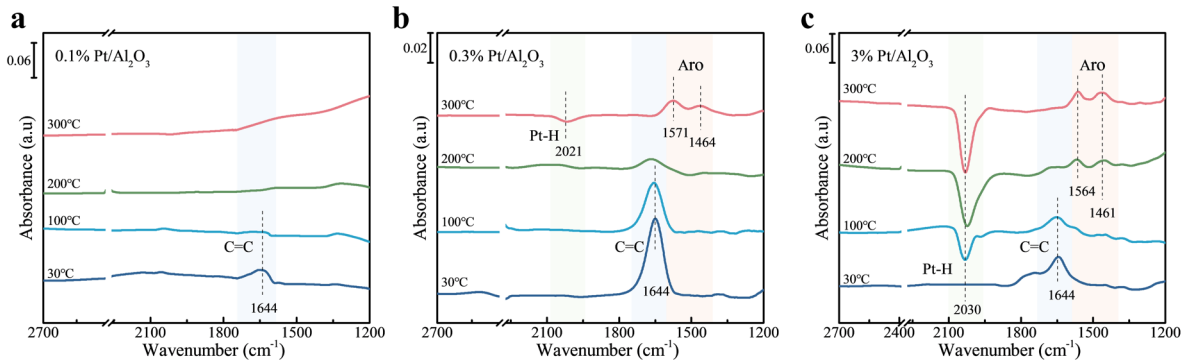

Figure 6. DRIFTS of C_3H_6 adsorption on the catalysts at different temperatures (a) 0.1% Pt/Al_2O_3, (b) 0.3% Pt/Al_2O_3 and (c) 3% Pt/Al_2O_3 catalysts.

Table 3. Pre-exponential factor and entropy changes of Pt/Al_2O_3 catalysts.

Catalyst	Activation energy [kJ/mol]	Pre-exponential factor [s^{-1}]	Entropy change [J/(mol·K)]
0.1% Pt/Al_2O_3	26 ± 3	2.65×10^5	-158.1
0.3% Pt/Al_2O_3	41 ± 5	4.51×10^6	-134.5
3% Pt/Al_2O_3	56 ± 6	1.25×10^7	-126.0

Zhao et al.[38] report the Pt single atom having the most positive charges by transferring charge to support is the most active, as evidence by comparing the first and second C-H bond activation energies in PDH, and has a good selectivity due to the higher activation energy for deep dehydrogenation than that for desorption of propylene. Therefore, it is reasonable to deduce that the superior catalytic activity of the atomically dispersed Pt/Al_2O_3 is attributable to the exposure of increased effective active sites, positively charged $Pt^{\delta+}$ centres. Those sites could enhance propane adsorption and facilitate the C-H bond activation, compared to small clusters and nanoparticles.

The relative adsorption strength of propylene on catalysts relates directly to the selectivity. The faster propylene desorption compared to the propylene dehydrogenation is preferred to get a high selectivity.[8,9] The size dependence of the propylene adsorption was characterized by the DRIFTS measurements and the results were given in Figure 6. The peaks at 1644 cm^{-1} can be assigned to the characteristic band of C=C stretching of propylene, and two peaks at 1570 and 1460 cm^{-1} are ascribed to the skeleton vibrations of the aromatics ring.[64,65] At a temperature of 30 °C, an absorption peak of the C=C stretching band at 1644 cm^{-1} is observed on all three catalysts. For 0.1% Pt/Al_2O_3, this peak almost disappears immediately after raising the temperature, and no new peaks appear. However, for 0.3% Pt/Al_2O_3 and 3% Pt/Al_2O_3, this peak is initially weakened before it disappears entirely at 300 °C, meanwhile an absorption peak of the aromatics ring appears. This indicates that the adsorption strength of propylene on 0.1% Pt/Al_2O_3 is relatively weak, and absorbed propylene on 0.1% Pt/Al_2O_3 tends to desorb more readily rather than that on 0.3% Pt/Al_2O_3 and 3% Pt/Al_2O_3. In addition, a derivative-shaped peak around 2020 cm^{-1} (caused by the surface Pt-H groups) is observed for 0.3% Pt/Al_2O_3 and 3% Pt/Al_2O_3 under higher temperatures.[66] The presence of Pt-H groups is associated with the deep dehydrogenation of propylene, and the relative intensity of the Pt-H band increases alongside increasing amounts of aromatic coke, suggesting that the formation of aromatic coke may be a direct result of deep dehydrogenation.[10] These results clearly indicate that weakened propylene adsorption on the atomically dispersed 0.1% Pt/Al_2O_3 catalyst facilitates desorption rather than deep dehydrogenation, thus leading to higher levels of selectivity compared to 0.3% Pt/Al_2O_3 sub-nano-catalyst and 3% Pt/Al_2O_3 nano-catalyst. This is also consistent with Furukawa et al.'s work, which indicates that the single-atom-like Pt well catalyzes the first and second C-H activation, while effectively inhibits the third one, which minimizes the side reactions to coke and improves the selectivity and stability.[37]

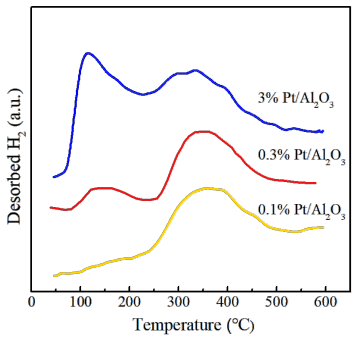

Figure 7. H_2-TPD profiles of the fresh 0.1% Pt/Al_2O_3, 0.3% Pt/Al_2O_3 and 3% Pt/Al_2O_3 catalysts.

In addition, H_2-TPD was also carried out and the results were presented in Figure 7. In general, low-temperature desorption peak (~100 °C) is assigned to hydrogen on metallic Pt, whereas high-temperature desorption peaks (300~450 °C) corresponds to spillover hydrogen.[57] In comparison with The 0.3% Pt/Al_2O_3 and 3% Pt/Al_2O_3 catalysts, the low-temperature desorption peak on 0.1% Pt/Al_2O_3 catalyst disappears and there only exists a high-temperature spillover hydrogen peak, suggesting that the metallic Pt is virtually nonexistent. Although the mechanism of the increase in hydrogen spillover with the decrease of Pt particle size is unclear, previous studies have shown that the high temperature adsorbed hydrogen aids in maintaining catalyst activity, most probably by reducing coking on the metal, and the surface sites where the spillover hydrogen and propane react cannot break C-C bonds.[67-70] Therefore, the enormous generation of spillover hydrogen on 0.1% Pt/Al_2O_3 could favor to reduce the coking on the surface and further increase the selectivity and stability of catalyst.

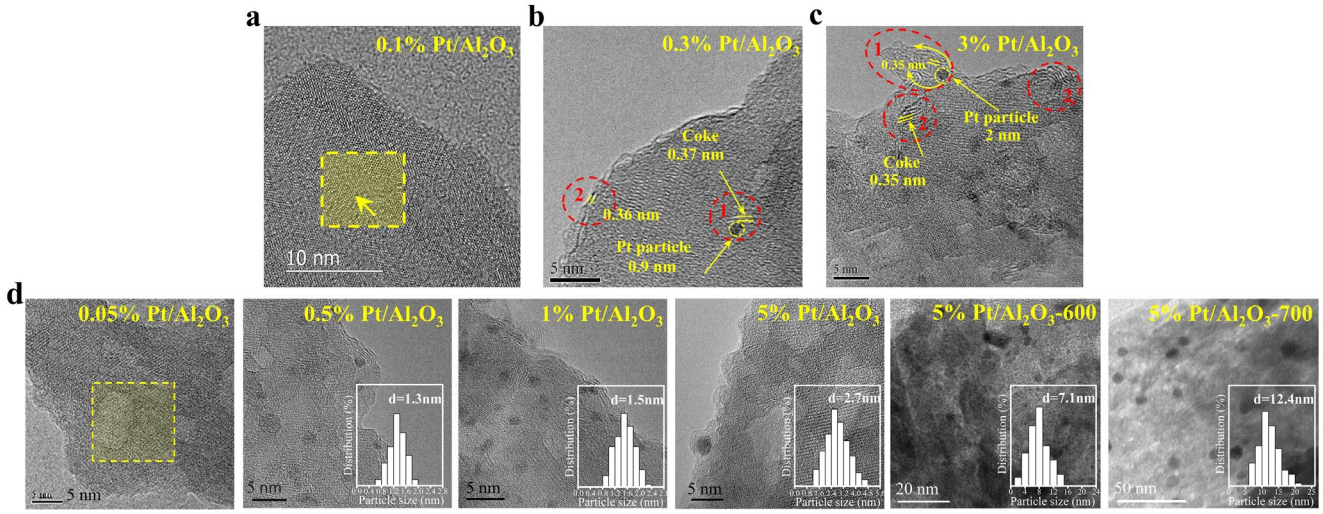

Figure 8. Typical TEM images of the representative multimetric Pt/Al_2O_3 catalysts, after 4 h of PDH reaction: (a) 0.1% Pt/Al_2O_3, (b) 0.3% Pt/Al_2O_3 , (c) 3% Pt/Al_2O_3, and (d) the spent Pt/Al_2O_3 catalysts in different sizes.

The Size Effects on Coke Properties and Catalyst Stability. The deactivation of Pt-based catalysts for PDH mainly originates from the formation of coke, an analysis procedure was performed to obtain comprehensive information about the size effects on coke properties. Figure 8 illustrate the typical TEM images of the spent Pt/Al_2O_3 in different scale. The Pt particle sizes of spent catalysts are presented in Table 1. There are no observable Pt nanoparticles on the spent 0.1% Pt/Al_2O_3, which verifies the supported Pt still maintains highly dispersed after reaction. The crystal lattice of carbon can barely be observed on 0.1% Pt/Al_2O_3 and become obvious when the amount of coke deposits increase with the increase of Pt loading. For 0.3% Pt/Al_2O_3 and 3% Pt/Al_2O_3 catalysts, the coke sheets attached to the metal particles (label 1) can be easily detected. The spacing lattice values of coke were measured as approximately 3.5-3.7 Å, which is larger than that of graphite (i.e., 3.35 Å). Thus, this coke on the catalyst could be pregraphite carbon.[71] It's well known that these carbonaceous species highly deficient in hydrogen are produced on the metal surface with multiple Pt-Pt sites.[72] That's the possible reason why no such kind of coke is produced on the 0.1% Pt/Al_2O_3 sample. With more pregraphite carbon accumulated on the Pt surface, it can expand from the surface to the support (label 2). The transfer of coke from Pt surface to the support is also reported in the literature and could be fastened when mobile species, e.g. Sn, exist in the catalyst.[10]

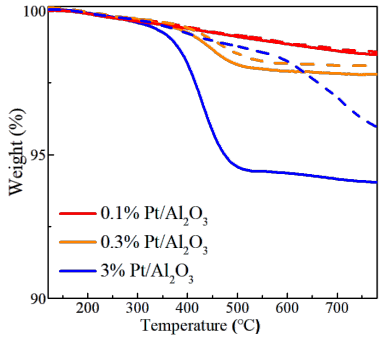

Figure 9. TG curves of the spent Pt/Al_2O_3 catalysts with different loading, O_2 atmosphere (— solid line), N_2 atmosphere (- - - dash line).

Table 4. Coking properties of the spent Pt/Al_2O_3 catalysts collected.

Sample[a]	Coke content-O_2[b] (wt%)	Coke content-N_2[c] (wt%)
0.1% Pt/Al_2O_3	1.5	1.5
0.3% Pt/Al_2O_3	2.2	1.8
3% Pt/Al_2O_3	5.9	4.2

[a] condition: 575 °C, reaction time 4 h. [b,c] Determined by TG in O_2 and N_2 atmosphere, respectively.

The amount of deposited coke were quantitatively determined by TG in an oxidizing and nitrogen atmosphere, respectively. The discrepancy of weight loss between O_2 and N_2 is due to the nonvolatile pregraphite-like carbon, which can be easily gasified in O_2 rather than in N_2, as previously reported.[10] Figure 9 shows that the weight loss of the spent 0.1% Pt/Al_2O_3 catalyst is the lowest (ca. 1.5 wt%) in the O_2 atmosphere, and the difference of weight loss between O_2 and N_2 is negligible. Increasing the Pt loading contributes to a higher amount of coke deposits and nonvolatile pregraphite-like carbon, this result also confirms with the results of TEM.

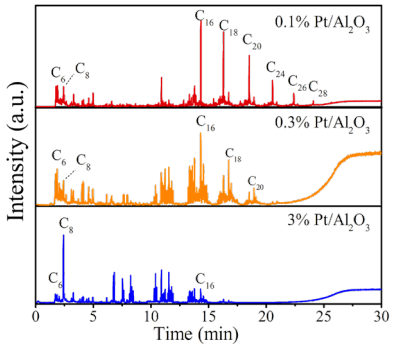

Figure 10. Pyrolysis GC-MS image of the spent Pt/Al_2O_3 catalysts with different loading.

Pyrolysis GC-MS analysis was further carried out to identify the composition of coke (Figure 10). When compared with 0.3% Pt/Al_2O_3 and 3% Pt/Al_2O_3, the retention time of main peaks in 0.1% Pt/Al_2O_3 significantly prolonged, indicating the

production of the longer-chain volatile aliphatic coke (C16-C26) due to the lack of multiple Pt-Pt sites.[10]

The multiple Pt-Pt sites existing in Pt-based catalysts are known to be active for deep dehydrogenation of propylene, cracking and the subsequent secondary reaction of the coke (e.g. isomerization, cyclization, etc.).[1,73,74] The selectivity and stability of catalyst depend on the balance between whether the product propylene directly desorbs or undergoes those undesired side reactions. When Pt particles achieve atomic-level dispersion, the multiple Pt-Pt sites basically disappear, and the relatively separate Pt atoms can effectively inhibit these undesired side reactions.[75-77] Therefore, the propene selectivity increases and the coking rate decreases.

CONCLUSION

The activity, selectivity, and stability were found to depend significantly on the Pt size. The dependence can be divided into three groups from the atomically dispersed, small clusters, and nanoparticles. The result indicates that when Pt particle size is reduced to subnanometer sized clusters (< 1 nm), in particular, when Pt particles achieve atomic-level dispersion, the highly dispersed Pt/Al_2O_3 catalyst exhibits a superior catalytic performance while still retaining a high propylene selectivity and stability, this is a distinguishing feature differ from the traditional nano-catalyst. The superior performance could be attributed to positively charged platinum centers that favor the preferential adsorption of propane. Meanwhile, instead of over-dehydrogenating, the propylene adsorbed on the atomically dispersed Pt/Al_2O_3 catalyst preferred to desorb. Resultantly, the selectivity of propylene improved.

Additionally, the absence of multiple Pt-Pt sites resulted in effectively inhibiting C-C cracking that requires the combination of multiple Pt atoms, which improved the propylene selectivity and anti-coking. In conclusion, the current work has systematically expatiated the size dependence of Pt/Al_2O_3 catalysts for propane dehydrogenation: from atomically dispersed to small clusters and then to nanoparticles. The result indicates that the atomically dispersed Pt/Al_2O_3 catalyst is a novel and much more effective catalyst for propane dehydrogenation with minimal use of noble metal, which possesses enormous potential for the industrial application.

AUTHOR INFORMATION

Corresponding Author

*E-mail: zhjsui@ecust.edu.cn.
*E-mail: de.chen@ntnu.no.

Author Contributions

‡These authors contributed equally.

Notes

The authors declare no competing financial interest.

ACKNOWLEDGMENT

This work was funded by National Key R&D Program of China (2018YFB0604700) and Natural Science Foundation of China (NSFC, 91645122). The authors thank Song Hong (Beijing University of Chemical and Technology) for his assistance with the transmission electron microscopy. The authors also thank Hongfei Ma (Norwegian University of Science and Technology) for the fruitful discussions.

REFERENCES

(1) Sattler, J. J. H. B.; Javier, R. M.; Eduardo, S. J.; Weckhuysen, B. M., Catalytic Dehydrogenation of Light Alkanes on Metals and Metal Oxides. *Chem. Rev.* **2014,** *114* (20), 10613-10653.

(2) Nawaz, Z., Light Alkane Dehydrogenation to Light Olefin Technologies: A Comprehensive Review. *Rev. Chem. Eng.* **2015,** *31* (5), 413-436.

(3) Searles, K.; Chan, K. W.; Burak, J. A. M.; Zemlyanov, D.; Safonova, O.; Coperet, C., Highly Productive Propane Dehydrogenation Catalyst Using Silica-Supported Ga-Pt Nanoparticles Generated from Single-Sites. *J. Am. Chem. Soc.* **2018,** *140* (37), 11674-11679.

(4) Xu, Z.; Yue, Y.; Bao, X.; Xie, Z.; Zhu, H., Propane Dehydrogenation over Pt Clusters Localized at the Sn Single-Site in Zeolite Framework. *ACS Catal.* **2020,** *10* (1), 818-828.

(5) Zhao, X.; Chen, S.; Fang, Z.; Ding, J.; Sang, W.; Wang, Y.; Zhao, J.; Peng, Z.; Zeng, J., Octahedral Pd@$Pt_{1.8}$Ni Core-Shell Nanocrystals with Ultrathin PtNi Alloy Shells as Active Catalysts for Oxygen Reduction Reaction. *J. Am. Chem. Soc.* **2015,** *137* (8), 2804-2807.

(6) Yu, C.; Xu, H.; Ge, Q.; Li, W., Properties of the Metallic Phase of Zinc-Doped Platinum Catalysts for Propane Dehydrogenation. *J. Mol. Catal. A: Chem.* **2007,** *266* (1), 80-87.

(7) Iglesias-Juez, A.; Beale, A. M.; Maaijen, K.; Weng, T. C.; Glatzel, P.; Weckhuysen, B. M., A Combined in Situ Time-Resolved UV-Vis, Raman and High-Energy Resolution X-ray Absorption Spectroscopy Study on the Deactivation Behavior of Pt and PtSn Propane Dehydrogenation Catalysts Under Industrial Reaction Conditions. *J. Catal.* **2010,** *276* (2), 268-279.

(8) Nykänen, L.; Honkala, K., Selectivity in Propene Dehydrogenation on Pt and Pt_3Sn Surfaces from First Principles. *ACS Catal.* **2013,** *3* (12), 3026-3030.

(9) Yang, M.; Zhu, Y.; Zhou, X.; Sui, Z.; Chen, D., First-Principles Calculations of Propane Dehydrogenation over PtSn Catalysts. *ACS Catal.* **2012,** *2* (6), 1247-1258.

(10) Wang, H.; Sun, L.; Sui, Z.; Zhu, Y.; Ye, G.; Chen, D.; Zhou, X.; Yuan, W., Coke Formation on Pt-Sn/Al_2O_3 Catalyst for Propane Dehydrogenation. *Ind. Eng. Chem. Res.* **2018,** *57* (26), 8647-8654.

(11) Han, Z.; Li, S.; Jiang, F.; Wang, T.; Ma, X.; Gong, J., Propane Dehydrogenation over Pt-Cu Bimetallic Catalysts: The Nature of Coke Deposition and the Role of Copper. *Nanoscale* **2014,** *6* (17), 10000-10008.

(12) Li, Q.; Sui, Z.; Zhou, X.; Zhu, Y.; Chen, D., Coke Formation on Pt-Sn/Al_2O_3 Catalyst in Propane Dehydrogenation: Coke Characterization and Kinetic Study. *Top. Catal.* **2011,** *54* (13-15), 888-896.

(13) Martin, N.; Viniegra, M.; Lima, E., Coke Characterization on Pt/Al_2O_3-β-Zeolite Reforming Catalysts. *Ind. Eng. Chem. Res.* **2004,** *43* (5), 1206-1210.

(14) Feng, J.; Liang, Z.; Li, S.; Gang, L.; Wang, S.; Gong, J., Propane Dehydrogenation over Pt/TiO_2-Al_2O_3 Catalysts. *ACS Catal.* **2015,** *5* (1), 438-447.

(15) Shan, Y.; Wang, T.; Sui, Z.; Zhu, Y.; Zhou, X., Hierarchical $MgAl_2O_4$ Supported Pt-Sn as a Highly Thermostable Catalyst for Propane Dehydrogenation. *Catal. Commun.* **2016,** *84*, 85-88.

(16) Santhosh K. M.; Chen, D.; Walmsley, J. C.; Holmen, A., Dehydrogenation of Propane over Pt-SBA-15: Effect of Pt Particle Size. *Catal. Commun.* **2008,** *9* (5), 747-750.

(17) Deng, L.; Miura, H.; Shishido, T.; Wang, Z.; Hosokawa, S.; Teramura, K.; Tanaka, T., Elucidating Strong Metal-Support Interactions in Pt-Sn/SiO_2 Catalyst and Its Consequences for Dehydrogenation of Lower Alkanes. *J. Catal.* **2018,** *365*, 277-291.

(18) Xu, Y.; Chen, J.; Yuan, X.; Zhang, Y.; Yu, J.; Liu, H.; Cao, M.; Fan, X.; Lin, H.; Zhang, Q., Sintering-Resistant Pt on Ga_2O_3 Rods for Propane Dehydrogenation: The Morphology Matters. *Ind. Eng. Chem. Res.* **2018,** *57* (39), 13087-13093.

(19) Zhu, J.; Yang, M.; Yu, Y.; Zhu, Y.; Sui, Z.; Zhou, X.; Holmen, A.; Chen, D., Size-Dependent Reaction Mechanism and Kinetics for Propane Dehydrogenation over Pt Catalysts. *ACS Catal.* **2015,** *5* (11), 6310-6319.

(20) Yang, M.; Zhu, Y.; Fan, C.; Sui, Z.; Chen, D.; Zhou, X., DFT Study of Propane Dehydrogenation on Pt Catalyst: Effects of Step Sites. *Phys. Chem. Chem. Phys.* **2011,** *13* (8), 3257-3267.

(21) Yang, M.; Zhu, J.; Zhu, Y.; Sui, Z.; Yu, Y.; Zhou, X.; Chen, D., Tuning Selectivity and Stability in Propane Dehydrogenation by

Shaping Pt Particles: A Combined Experimental and DFT Study. *J. Mol. Catal. A: Chem.* **2014,** *395*, 329-336.

(22) Yang, X.; Wang, A.; Qiao, B.; Li, J.; Liu, J.; Zhang, T., Single-Atom Catalysts: A New Frontier in Heterogeneous Catalysis. *Acc. Chem. Res.* **2013,** *46* (8), 1740-1748.

(23) Shi, Y.; Zhao, C.; Wei, H.; Guo, J.; Liang, S.; Wang, A.; Tao, Z.; Liu, J.; Ma, T., Single-Atom Catalysis in Mesoporous Photovoltaics: The Principle of Utility Maximization. *Adv. Mater.* **2014,** *26* (48), 8147-8153.

(24) Qiao, B.; Wang, A.; Yang, X.; Zhang, T., Single-Atom Catalysis of CO Oxidation Using Pt_1/FeO_x. *Nat. Chem.* **2011,** *3* (8), 634-641.

(25) Lang, R.; Xi, W.; Liu, J. C.; Cui, Y. T.; Li, T.; Lee, A. F.; Chen, F.; Chen, Y.; Li, L.; Lin, J.; Miao, S.; Liu, X.; Wang, A.; Wang, X.; Luo, J.; Qiao, B.; Li, J.; Zhang, T., Non-Defect-Stabilized Thermally Stable Single-Atom Catalyst. *Nat. Commun.* **2019,** *10* (1), 1-10.

(26) Lu, J.; Aydin, C.; Browning, N.; Gates, B., Imaging Isolated Gold Atom Catalytic Sites in Zeolite Nay. *Angew. Chem.* **2012,** *124* (24), 5944-5948.

(27) Ren, Y.; Tang, Y.; Zhang, L.; Liu, X.; Li, L.; Miao, S.; Su, D.; Wang, A.; Li, J.; Zhang, T., Unraveling the Coordination Structure-Performance Relationship in Pt_1/Fe_2O_3 Single-Atom Catalyst. *Nat. Commun.* **2019,** *10* (1), 1-9.

(28) Zhang, Z.; Zhu, Y.; Asakura, H.; Zhang, B.; Zhang, J.; Zhou, M.; Han, Y.; Tanaka, T.; Wang, A.; Zhang, T., Thermally Stable Single Atom Pt/m-Al_2O_3 for Selective Hydrogenation and CO Oxidation. *Nat. Commun.* **2017,** *8(1)*, 1-10.

(29) Qiao, B.; Wang, A.; Yang, X.; Allard, L.; Jiang, Z.; Cui, Y.; Liu, J.; Li, J.; Zhang, T., Single-Atom Catalysis of CO Oxidation Using Pt_1/FeO_x. *Nat. Chem.* **2011,** *3* (8), 634-641.

(30) Wei, H.; Liu, X.; Wang, A.; Zhang, T., FeO_x-Supported Platinum Single-Atom and Pseudo-Single-Atom Catalysts for Chemoselective Hydrogenation of Functionalized Nitroarenes. *Nat. Commun.* **2014,** *5* (1), 5634.

(31) Ding, K.; Gulec, A.; Johnson, A.; Schweitzer, N.; Stucky, G.; Marks, L.; Stair, P., Identification of Active Sites in CO Oxidation and Water-Gas Shift over Supported Pt Catalysts. *Sci.* **2015,** *350* (6257), 189-192.

(32) Liang, J.; Jian, L.; Yang, X.; Wang, A.; Qiao, B.; Liu, J.; Tao, Z.; Li, J., Theoretical and Experimental Investigations on Single-Atom Catalysis: Ir_1/FeO_x for CO oxidation. *J. Phys. Chem. C* **2014,** *118* (1), 21945-21951.

(33) Lin, L.; Zhou, W.; Gao, R.; Yao, S.; Zhang, X.; Xu, W.; Zheng, S.; Jiang, Z.; Yu, Q.; Li, Y., Low-Temperature Hydrogen Production from Water and Methanol Using Pt/α-MoC Catalysts. *Nat.* **2017,** *544* (7648), 80-83.

(34) Yang, S.; Kim, J.; Tak, Y.; Soon, A.; Lee, H., Single-Atom Catalyst of Platinum Supported on Titanium Nitride for Selective Electrochemical Reactions. *Angew. Chem. Int. Ed.* **2016,** *55* (6), 2058-2062.

(35) Tao, H.; Choi, C.; Ding, L.; Jiang, Z.; Han, Z.; Jia, M.; Fan, Q.; Gao, Y.; Wang, H.; Robertson, A., Nitrogen Fixation by Ru Single-Atom Electrocatalytic Reduction. *Chem* **2019,** *5* (1), 204-214.

(36) Sun, G.; Zhao, Z.; Mu, R.; Zha, S.; Li, L.; Chen, S.; Zang, K.; Luo, J.; Li, Z.; Purdy, S.; Kropf, A.; Miller, J.; Zeng, L.; Gong, J., Breaking the Scaling Relationship via Thermally Stable Pt/Cu Single Atom Alloys for Catalytic Dehydrogenation. *Nat. Commun.* **2018,** *9* (1), 1-9.

(37) Nakaya, Y.; Hirayama, J.; Yamazoe, S.; Shimizu, K.; Furukawa, S., Single-Atom Pt in Intermetallics as an Ultrastable and Selective Catalyst for Propane Dehydrogenation. *Nat. Commun.* **2020,** *11* (1), 1-7.

(38) Sun, X.; Han, P.; Li, B.; Zhao, Z., Tunable Catalytic Performance of Single Pt Atom on Doped Graphene in Direct Dehydrogenation of Propane by Rational Doping: A Density Functional Theory Study. *J. Phys. Chem. C* **2018,** *122* (3), 1570-1576.

(39) Sun, Y.; Wang, H.; Li, P.; Duan, X.; Xu, J.; Han, Y., Synthesis and Identification of Hierarchical γ-AlOOH Self-Assembled by Nanosheets with Adjustable Exposed Facets. *CrystEngComm* **2016,** *18* (24), 4546-4554.

(40) Yoo, E.; Okata, T.; Akita, T.; Kohyama, M.; Nakamura, J.; Honma, I., Enhanced Electrocatalytic Activity of Pt Subnanoclusters on Graphene Nanosheet Surface. *Nano Lett.* **2009,** *9* (6), 2255-2259.

(41) Kumar, M.; Chen, D.; Holmen, A.; Walmsley, J., Dehydrogenation of Propane over Pt-SBA-15 and Pt-Sn-SBA-15: Effect of Sn on the Dispersion of Pt and Catalytic Behavior. *Catal. Today* **2009,** *142* (1-2), 17-23.

(42) Salmones, J.; Wang, J. A.; Galicia, J. A.; Aguilar-Rios, G., H_2 Reduction Behaviors and Catalytic Performance of Bimetallic Tin-Modified Platinum Catalysts for Propane Dehydrogenation. *J. Mol. Catal. A: Chem.* **2002,** *184* (1-2), 203-213.

(43) Waku, T.; Biscardi, J. A.; Iglesia, E., Active, Selective, and Stable Pt/Na-[Fe]ZSM5 Catalyst for the Dehydrogenation of Light Alkanes. *Chem. Commun.* **2003,** *14,* 1764-1765.

(44) Cola, P.; Glaser, R.; Weitkamp, J., Non-Oxidative Propane Dehydrogenation over Pt-Zn-Containing Zeolites. *Appl. Catal. A: Gen.* **2006,** *306*, 85-97.

(45) Siddiqi, G.; Sun, P.; Galvita, V.; Bell, A. T., Catalyst Performance of Novel Pt/Mg(Ga)(Al)O Catalysts for Alkane Dehydrogenation. *J. Catal.* **2010,** *274* (2), 200-206.

(46) Duan, Y.; Zhou, Y.; Zhang, Y.; Sheng, X.; Zhou, S.; Zhang, Z., Effect of Aluminum Modification on Catalytic Properties of PtSn-Based Catalysts Supported on SBA-15 for Propane Dehydrogenation. *J. Nat. Gas Chem.* **2012,** *141* (1), 120-127.

(47) Sun, P.; Siddiqi, G.; Vining, W.; Chi, M.; Bell, A., Novel Pt/Mg(In)(Al)O Catalysts for Ethane and Propane Dehydrogenation. *J. Catal.* **2011,** *282* (1), 165-174.

(48) Zhu, H.; Anjum, D. H.; Wang, Q.; Abou-Hamad, E.; Emsley, L.; Dong, H.; Laveille, P.; Li, L.; Samal, A.; Basset, J., Sn Surface-Enriched Pt-Sn Bimetallic Nanoparticles as a Selective and Stable Catalyst for Propane Dehydrogenation. *J. Catal.* **2014,** *320*, 52-62.

(49) Deng, L.; Shishido, T.; Teramura, K.; Tanaka, T., Effect of Reduction Method on the Activity of Pt-Sn/SiO_2 for Dehydrogenation of Propane. *Catal. Today* **2014,** *232*, 33-39.

(50) Xia, K.; Lang, W. Z.; Li, P.; Yan, X.; Guo, Y., The Properties and Catalytic Performance of PtIn/Mg(Al)O Catalysts for the Propane Dehydrogenation Reaction: Effects of pH Value in Preparing Mg(Al)O Supports by the Co-precipitation Method. *J. Catal.* **2016,** *338*, 104-114.

(51) Liu, J.; Yue, Y.; Liu, H.; Da, Z.; Liu, C.; Ma, A.; Rong, J.; Su, D.; Bao, X.; Zheng, H., Origin of the Robust Catalytic Performance of Nanodiamond-Graphene-Supported Pt Nanoparticles Used in the Propane Dehydrogenation Reaction. *ACS Catal.* **2017,** *7* (5), 3349-3355.

(52) Xiong, H.; Lin, S.; Goetze, J.; Pletcher, P.; Datye, A., Thermally Stable and Regenerable Pt-Sn Clusters for Propane Dehydrogenation Prepared via Atom Trapping on Ceria. *Angew. Chem. Int. Ed.* **2017,** *56* (31), 8986-8991.

(53) Ren, G.; Pei, G.; Ren, Y.; Liu, K.; Chen, Z.; Yang, J.; Su Y.; Liu X.; Li W.; Zhang, T., Effect of Group IB Metals on the Dehydrogenation of Propane to Propylene over Anti-sintering Pt/$MgAl_2O_4$. *J. Catal.* **2018,** *366*, 115-126.

(54) Liu, J.; Li, J.; Rong, J.; Liu, C.; Dai, Z.; Bao, J.; Zheng, H., Defect-driven Unique Stability of Pt/Carbon Nanotubes for Propane Dehydrogenation. *Appl. Surf. Sci.* **2019,** *464*, 146-152.

(55) Wang, Y.; Hu, Z.; Tian, W.; Gao, L.; Yuan, Z., Framework-confined Sn in Si-Beta Stabilizing Ultra-small Pt Nanoclusters as Direct Propane Dehydrogenation Catalysts with High Selectivity and Stability. *Catal. Sci. Technol.* **2019,** *9* (24), 6993-7002.

(56) Wang, Y.; Hu, Z.; Lv, X.; Chen, L.; Yuan, Z., Ultrasmall PtZn Bimetallic Nanoclusters Encapsulated in Silicalite-1 Zeolite with Superior Performance for Propane Dehydrogenation. *J. Catal.* **2020,** *385*, 61-69.

(57) Zhang, Y.; Zhou, Y.; Huang, L.; Xue, M.; Zhang, S., Sn-Modified ZSM-5 as Support for Platinum Catalyst in Propane Dehydrogenation. *Ind. Eng. Chem. Res.* **2011,** *50* (13), 7896-7902.

(58) Navarro, R.; Alvarez-Galvan, M.; Sanchez-Sanchez, M.; Rosa, F.; Fierro, J., Production of Hydrogen by Oxidative Reforming of Ethanol over Pt Catalysts Supported on Al_2O_3 Modified with Ce and La. *Appl. Catal. B* **2005,** *55* (4), 229-241.

(59) Riguetto, B.; Damyanova, S.; Gouliev, G.; Marques, C.; Petrov, L.; Bueno, J., Surface Behavior of Alumina-Supported Pt Catalysts Modified with Cerium as Revealed by X-Ray Diffraction, X-Ray

Photoelectron Spectroscopy, and Fourier Transform Infrared Spectroscopy of CO Adsorption. *J. Phys. Chem. B* **2004,** *108* (17), 5349-5358.

(60) Serrano-Ruiz, J.; Huber, G.; Sánchez-Castillo, M.; Dumesic, J.; Rodríguez-Reinoso, F.; Sepúlveda-Escribano, A., Effect of Sn Addition to Pt/CeO_2-Al_2O_3 and Pt/Al_2O_3 Catalysts: An XPS, ^{119}Sn Mössbauer and Microcalorimetry Study. *J. Catal.* **2006,** *241* (2), 378-388.

(61) Kale, M.; Christopher, P., Utilizing Quantitative in Situ FTIR Spectroscopy to Identify Well-Coordinated Pt Atoms as the Active Site for CO Oxidation on Al_2O_3-Supported Pt Catalysts. *ACS Catal.* **2016,** *6* (8), 5599-5609.

(62) Chen, W.; Li, D.; Peng, C.; Qian, G.; Duan, X.; Chen, D.; Zhou, X., Mechanistic and Kinetic Insights into the Pt-Ru Synergy During Hydrogen Generation from Ammonia Borane over PtRu/CNT Nanocatalysts. *J. Catal.* **2017,** *356*, 186-196.

(63) Wang, H.; Blaylock, D.; Dam, A.; Liland, S.; Rout, K.; Zhu, Y.; Green, W.; Holmen, A.; Chen, D., Steam Methane Reforming on a Ni-based Bimetallic Catalyst: Density Functional Theory and Experimental Studies of the Catalytic Consequence of Surface Alloying of Ni with Ag. *Catal. Sci. Technol.* **2017,** *7* (8), 1713-1725.

(64) Amakawa, K.; Wrabetz, S.; Kroehnert, J.; Tzolova-Mueller, G.; Schloegl, R.; Trunschke, A., In Situ Generation of Active Sites in Olefin Metathesis. *J. Am. Chem. Soc.* **2012,** *134* (28), 11462-11473.

(65) Meunier, F.; Zuzaniuk, V.; Breen, J.; Olsson, M.; Ross, J., Mechanistic Differences in the Selective Reduction of NO by Propene Over Cobalt- and Silver-Promoted Alumina Catalysts: Kinetic and in Situ Drifts Study. *Catal. Today* **2000,** *59* (3-4), 287-304.

(66) Ko, M.; Frei, H., Millisecond FT-IR Spectroscopy of Surface Intermediates of C_2H_4 Hydrogenation over Pt/Al_2O_3 Catalyst Under Reaction Conditions. *J. Phys. Chem. B* **2004,** *108* (6), 1805-1808.

(67) Yu, C.; Ge, Q.; Xu, H.; Li, W.; Yu, C.; Ge, Q.; Xu, H.; Li, W., Effects of Ce Addition on the Pt-Sn/Gamma-Al_2O_3 Catalyst for Propane Dehydrogenation to Propylene. *Appl. Catal. A: Gen.* **2006,** *315*, 58-67.

(68) Pajonk, G., Contribution of Spillover Effects to Heterogeneous Catalysis. *Appl. Catal. A: Gen* **2000,** *202* (2), 157-169.

(69) Im, J.; Shin, H.; Jang, H.; Kim, H.; Choi, M., Maximizing the Catalytic Function of Hydrogen Spillover in Platinum-Encapsulated Aluminosilicates with Controlled Nanostructures. *Nat. Commun.* **2014,** *5* (1), 1-8.

(70) Bariås, A.; Holmen, A.; Blekkan, A., Propane Dehydrogenation over Supported Pt and Pt-Sn Catalysts: Catalyst Preparation, Characterization, and Activity Measurements. *J. Catal.* **1996**, *158* (1), 1-12.

(71) Crespi, V., Microscopic Determination of the Interlayer Binding Energy in Graphite. *Chem. Phys. Lett.* **1998,** *286* (5-6), 490-496.

(72) Redekop, E.; Saerens, S.; Galvita, V.; González, I.; Sabbe, M.; Bliznuk, V.; Marin, G., Early Stages in the Formation and Burning of Graphene on a $Pt/Mg(Al)O_x$ Dehydrogenation Catalyst: A Temperature and Time Resolved Study. *J. Catal.* **2016,** *344*, 482-495.

(73) Hauser, A.; Horn, P.; Head-Gordon, M.; Bell, A., A Systematic Study on Pt Based, Subnanometer-Sized Alloy Cluster Catalysts for Alkane Dehydrogenation: Effects of Intermetallic Interaction. *PCCP* **2016,** *18* (16), 10906-10917.

(74) Zhao, Z.; Chiu, C.; Gong J., Molecular Understandings on the Activation of Light Hydrocarbons over Heterogeneous Catalysts. *Chem. Sci.* **2015,** *6* (8), 4403-4425.

(75) Seshan, K., Dehydrogenation of N-dodecane over PtSn/MgAlO Catalysts: Investigating the Catalyst Performance while Monitoring the Products. *Appl. Catal. A: Gen.* **2014,** *469*, 74-80.

(76) Bhasin, M.; Mccain, J.; Vora, B.; Imai, T., Dehydrogenation and Oxydehydrogenation of Paraffins to Olefins. *Appl. Catal. A: Gen.* **2001,** *221* (1-2), 397-419.

(77) Karimzadeh, R., Catalytic Cracking of Hydrocarbons over Modified ZSM-5 Zeolites to Produce Light Olefins: A Review. *Appl. Catal. A: Gen.* **2011,** *398* (1-2), 1-17.

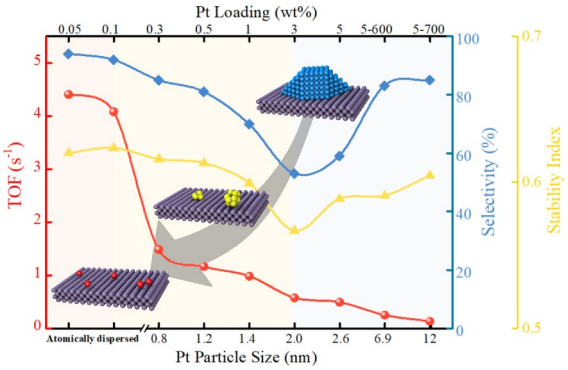
Pt Loading (wt%)
0.05
0.1
0.3
0.5
1
3
5
5-600
5-700
TOF (s^{-1})
Selectivity (%)
Stability Index
Atomically dispersed
0.8
1.2
1.4
2.0
2.6
6.9
12
Pt Particle Size (nm)